Distribution of Tritium in the Near Surface of Candidate Structural Materials for Fusion Reactors. Type 304L Stainless Steel, Inconel, Hastelloy, Eurofer-97, Oxide Dispersion-Strengthened Alloy 14YWT

James O'Callaghan, Walter T. Shmayda, Henry Smith, Matthew Sharpe, Lyn McWilliam, Philippa Almond, Rhiann Canavan, Nathan Eedy, Gowri Karajgikar, David Kennedy, Hazel Gardner, Fatimah Sanni, Alec Shackleford, Callum Steventon, Josh Ruby, Tshepo Mahafa, David. T. Hoelzer, Kalle Heinola, and Anthony Hollingsworth

***Abstract*— Five different candidate structural materials for fusion have undergone pure tritium gas soaking at room temperature and at 310-mbar(a) pressure. The tritium uptake on the surface and in the bulk of the alloys has been analyzed using surface leaching, chemical etching, and thermal desorption. The nickel-based alloys: Inconel-X-750 and Hastelloy-X, absorbed the least amount of total tritium compared with austenitic stainless steel AISI 304L, reduced activation ferritic-martensitic (RAFM) Eurofer-97, and advanced nanoferritic alloy 14YWT. Microstructural analyses using electron backscatter diffraction (EBSD) indicate that the number of grains and mean grain size is not a dominant factor in near surface tritium uptake. The quantity of iron dissolved in the surface oxide appears to be the major factor in encouraging tritium absorption.**

***Index Terms*— Stainless steel alloys, surface inventory, tritium absorption, tritium bulk profiles, tritium solubility, XPS.**

I. Introduction

TRITIUM accumulation and permeation into and throughout fusion relevant materials presents several challenges to fusion research and has the potential to affect various areas from waste management to tritium accountancy. Tritium has been shown to accumulate in materials in a different way to protium (^{1}H) and deuterium prior to steady-state permeation [1], [2], [3]. An increased knowledge of the distribution of tritium throughout fusion relevant metals will lead to increased understanding of tritium permeation, reaping a host of benefits, from improved material selection to more efficient waste treatments. To this end, United Kingdom Atomic Energy Authority (UKAEA) and the University of Rochester's Laboratory for Laser Energetics (UR LLE) have conducted a collaborative study to further LLE's work on tritium ingress into stainless steel 316L [4], [5], [6], [7], [8], [9] by investigating five different alloys. These metals are AISI 304L, Inconel X-750, Hastelloy-X, Eurofer-97, and oxide dispersion strengthened (ODS) alloy 14YWT. The experiment utilized chemical treatments to gain a better understanding of tritium profiles as a function of depth for the different metals. The analysis method consisted of three main steps: a zinc chloride wash, multiple acid etches, and thermal desorption. The zinc chloride wash aimed to remove all the surface bound tritium by undercutting the hydroxyl layer typically found at the metal oxide/surface interface. Etching aimed to investigate the tritium content as a function of depth. Finally, high-temperature desorption strove to measure the residual tritium inventory residing deep within the metal bulk.

Manuscript received 29 September 2023; revised 11 January 2024, 11 April 2024, and 22 April 2024; accepted 29 April 2024. This work was supported in part by the Department for Business, Energy and Industrial Strategy (BEIS) Tactical Fund Memorandum of Understanding (MOU1) and in part by the International Partnerships Fund. The review of this article was arranged by Senior Editor R. Chapman. *(Corresponding author: James O'Callaghan.)*

James O'Callaghan, Henry Smith, Lyn McWilliam, Philippa Almond, Rhiann Canavan, Nathan Eedy, Gowri Karajgikar, David Kennedy, Hazel Gardner, Fatimah Sanni, Alec Shackleford, Callum Steventon, Tshepo Mahafa, and Anthony Hollingsworth are with U.K. Atomic Energy Authority, Culham Campus, OX14 3DB Abingdon, U.K. (e-mail: james.ocallaghan@ukaea.uk).

Walter T. Shmayda is with Tritium Solutions Inc., Rochester, NY 14618 USA.

Matthew Sharpe and Josh Ruby are with the Laboratory for Laser Energetics, University of Rochester, Rochester, NY 14623 USA.

David. T. Hoelzer is with the Oak Ridge National Laboratory, Oak Ridge, TN 37830 USA.

Kalle Heinola is with International Atomic Energy Agency, 1400 Vienna, Austria.

Color versions of one or more figures in this article are available at https://doi.org/10.1109/TPS.2024.3396645.

Digital Object Identifier 10.1109/TPS.2024.3396645

II. Methods

A. Material Compositions

The materials selected for this study are candidates for use in fusion application. 304/304L is already widely used for tritium facing components often along with 316/316L. Eurofer-97 is a reduced activation ferritic martensitic steel (RAFM) and is therefore potentially useful in a high neutron flux environment. 14YWT is a nanostructured ferritic

TABLE I

APPROXIMATE PERCENTAGE (WT%) COMPOSITION OF EACH ALLOY (NOTE 14YWT BETTER CHARACTERIZED THAN OTHERS [12])

	Fe	*Ni*	*Cr*	*Mn*	*Si*	*Mo*	*W*	*Co*	*Ti*	*Nb*	*Y*	*Other*
AISI 304L	Bal.	10	18	2	1	-	-	-	-	-	-	<1
Eurofer 97	Bal.	-	9	0.4	-	-	1.1	-	-	-	-	<1
Inconel X-750	7	Bal.	15.5	-	-	-	-	-	2.5	1	-	<1
Hastelloy X	18	Bal.	21	-	<1	9	0.6	1.5	-	-	-	<1
14YWT	Bal.	n/a	14.3	0.008	0.043	n/a	2.32	n/a	0.27	n/a	0.19	<1

alloy developed at Oak Ridge National Laboratory (ORNL), designed for high radiation tolerance, to be used in high heat flux areas. Inconel X-750 and Hastelloy-X are nickel-based superalloys and are also candidates for use in fusion reactors. Full compositions are outlined in Table I.

B. Sample Preparation and Exposure to Tritium

The samples had dimensions 51 × 18 × 3 mm. Five samples of each material were polished on both major faces to a mirror finish using a colloidal silica suspension. Once polished, the samples were sonically degreased using acetone, rinsed with deionized water, and finally with isopropanol. It is important to note that these samples would have both their nanometer thick native oxide and adsorbed water layer re-established due to storage in lab air for a few days [10], [11]. This adsorbed water can usually be removed, asides from a few monolayers, by pulling a vacuum; however, from our results, it seems that this degassing was not as thorough as previous work [6], [8], [9].

The samples were exposed to 100% tritium at American Radiolabelled Chemicals for 24 h at room temperature (20 °C) in a stainless steel exposure chamber. The chamber was pressurized to 1000 mbar(a), but due to a leak, the pressure had decreased to 310 mbar(a) after 24 h.

C. Procedure for Determining Tritium Content

The procedure used in this experiment is a combination and refinement of work carried out by Tanaka et al. [13] to measure the surface inventories and by Penzhorn et al. [3] to measure tritium depth profiles. This study provides an in-depth overview of the location and concentration of tritium on the surface and throughout the sample. The procedure consists of three parts: a zinc chloride wash, followed by a series of chemical etches, and finally a thermal desorption. All solutions generated in this process are analyzed using liquid scintillation counting (LSC).

D. Zinc Chloride Wash

All structural materials have an adsorbed water layer on them (see Fig. 1). In the initial stages of tritium exposure, tritons rapidly replace protiums in this water layer to attain an equilibrium between the gas phase partial pressure and the tritium concentration in the water layer [3], [11], [14]. This water layer is key to the initial stages of tritium uptake by

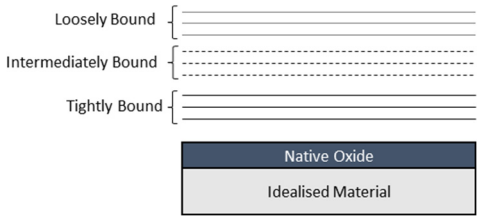

Fig. 1. Tritium uptake in non-idealised surfaces starts with substitutions of tritons into loosely bound surface adsorbed water, adapted from DOE report [14] and Thiel and Madey [15].

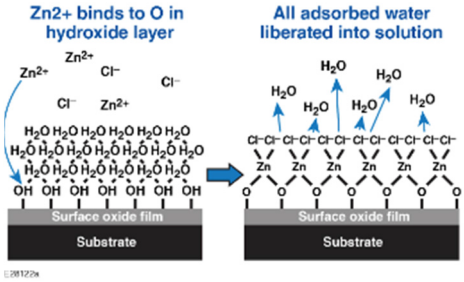

Fig. 2. Zinc chloride undercutting the hydroxyl layer adapted from Tanaka et al. [13].

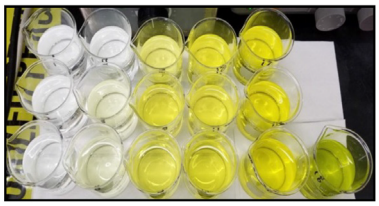

Fig. 3. Array of beakers containing acid and etchant. The color of the mixture intensifies with increasing etch time and acid concentration.

a material, by providing both a concentration gradient and reservoir of tritons.

Tanaka et al. [13] have shown zinc chloride to be an effective method of undercutting surface hydroxyl layers, removing tritium from the water layers found on the surface of materials. The addition of ZnCl solution to the metal forms a zinc complex on the surface by reacting with hydroxyl groups, as shown in Fig. 2. This binds the zinc to the oxygen, thereby releasing hydrogen ions, including any surface bound tritium.

This step is critical to understand the quantity of tritium present in the first surface layers of a material. It is known that most of the tritium is located near the surface, but there is limited data on the quantities and depth. Previous research conducted on stainless steel 316 at the University

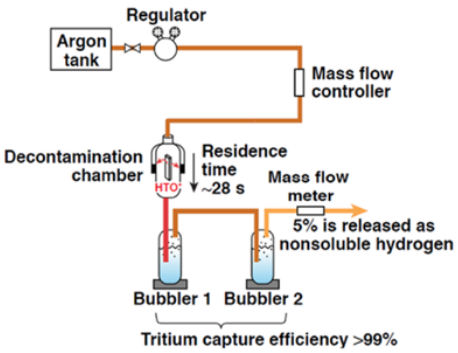

Fig. 4. Adapted from Fagan [9]. Cartoon of the thermal desorption facility, scintillation fluid is in bubbler one and water in bubbler two. Capture efficiency determined in previous works [17].

of Rochester [4], [5], [6], [7], [8], [9] has shown that as much as 40% (±20%) of a material's tritium inventory lies in the surface water layers found attached to the metal oxide despite dry storage.

The samples used in this experiment were submersed in a 50-mL 0.4M ZnCl solution for 5 min. Following sample removal, a 0.25-mL aliquot of the ZnCl solution was taken for LSC to determine tritium activity. The sample was then dried and transferred for acid etching.

E. Chemical Etching

As with previous works [4], [5], [6], [8], [9], [16], the acid etching procedure aims to probe the location and activity of tritium as a function of depth through the metal. With the use of multiple etches, a concentration profile can be deduced to determine the distribution of tritium as one proceeds deeper into the metal bulk (see Fig. 3).

The etches were completed using two different concentrations of aqua regia; 1/4 aqua regia with a ratio of 12:3:1 water:HCl:HNO_3 and 1/2 aqua regia with a ratio of 4:3:1 water:HCl:HNO_3; 17 etches were completed on each sample, using 60 mL of acid for each etch with the sample fully submerged during the process. This large number of etches provides a detailed concentration profile for the tritium present in the samples, leading to a greater understanding in the location of tritium throughout the sample.

Following each etch, the sample was washed with 8 mL of deionized water to quench the etching process. The water was added to the acid sample volume to capture the residual tritium in the acid on the metal surface. The sample was dried using nitrogen prior to mass measurement. The mass of the sample was recorded before and after each etch to determine the mass reduction and, assuming a homogenous etch, a depth etched can be calculated. The etches were completed at room temperature and utilized a stirring plate and magnetic stir rod to agitate the acid over the samples.

It should be noted that the etching procedure for Eurofer was altered. Due to its magnetic properties, a stir bar was unusable. A combination of hand stirring and ultrasonic bath was used to agitate the fluid over the metal surface. Early tests also revealed that Eurofer was significantly more corrodible, making the etch more challenging.

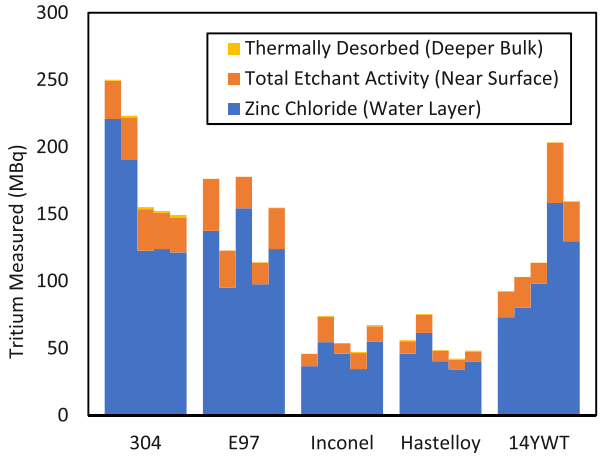

Fig. 5. Total tritium inventory retrieved from the five samples of each alloy 304 stainless steel, Eurofer 97, Inconel X-750, Hastelloy X, and 14YWT. The near surface here is the activity removed by the acid etching and can extend quite far into the material (see Fig. 6).

F. Thermal Desorption

Thermal desorption (see Fig. 4) was used after the chemical etching procedure to measure the residual tritium inventory remaining in the sample. Each sample was placed in an oven, which was ramped at 3 K/min to 793 K for a dwell of 4 h at temperature. Argon is flowed through the oven to purge desorbing tritium into a set of two bubblers, one bubbler containing 100 mL of liquid scintillation cocktail and the other 100 mL of deionized water. After the desorption, the activity of both fluids was counted.

G. Liquid Scintillation Counting

Liquid scintillation counts were taken using National Diagnostics' Ecosint H for the zinc chloride washes and the thermal desorption bubblers. For the acid etches, the solution was adjusted to pH 1 with the addition of 25% NaOH solution. This ensured that the scintillation cocktail did not cloud or scramble. Following this, a sample-to-liquid scintillation cocktail dilution of 1:17 was used. Ultima Gold LLT by PerkinElmer was chosen for its good performance in the presence of acids.

A color quench test was performed (see Table II) to quantify the impact of different colored solutions upon the measurement of the activity. An uncontaminated sample went through the etching procedure and a known quantity of tritium was spiked into each solution. The impact was negligible compared to pipetting accuracy.

III. Results

A. Tritium Depth Profiles

Fig. 5 provides the total tritium inventory collected from the alloys. Inconel and Hastelloy contain the lowest inventory of the five alloys investigated by a factor of two. As mentioned earlier, the high tritiated water layer indicates that the removal of water layer prior to tritium treatment was likely not as thorough as previous work [6], [8], [9].

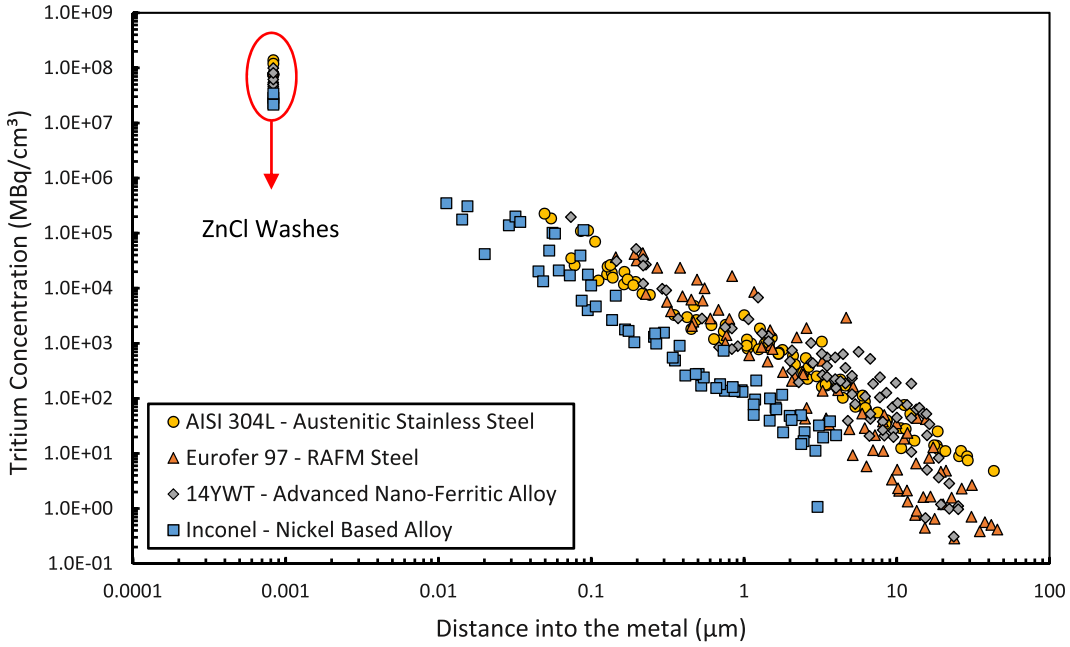

Fig. 6. Tritium concentration profile as a function of depth into the material for four alloys AISI 304Ll, Eurofer 97, Inconel X-750, and 14YWT. Concentrations of zinc chloride. Data at 0.828 μm are the zinc chloride aliquot based on the assumed depth of the water layer [5].

Fig. 6 shows the tritium depth profiles for this study generated by the zinc chloride wash and the chemical etching. Hastelloy X is not included in this figure because the etching process did not remove material evenly making it difficult to provide a meaningful tritium profile in the bulk.

The time taken between tritium exposure and depth profile measurement is not expected to play a significant role here [5], [8]. The somewhat large spread in data has been attributed to the statistical nature of tritium uptake. Errors due to pipetting and staff familiarity of method have been mostly eliminated. There has been a concerted effort to unravel the nature of this variability outlined and discussed in previous work [4], [5], [6], [7], [8], [9], which is unfortunately still not resolved.

Fig. 7 correlates tritium bound in the adsorbed water layer with the tritium inventory beyond; in what we have labeled "near surface." Both Inconel and Hastelloy have the lowest tritium inventories, while AISI 304L and Eurofer have the highest when averaged over the five samples in each group. There appears to be a correlation between the tritium content resident on the surface and the total tritium inventory, with both Inconel and Hastelloy having the lowest quantities of surface bound tritium. Both alloys have the lowest iron content, which suggests reduced iron hydroxide complexes on the surface.

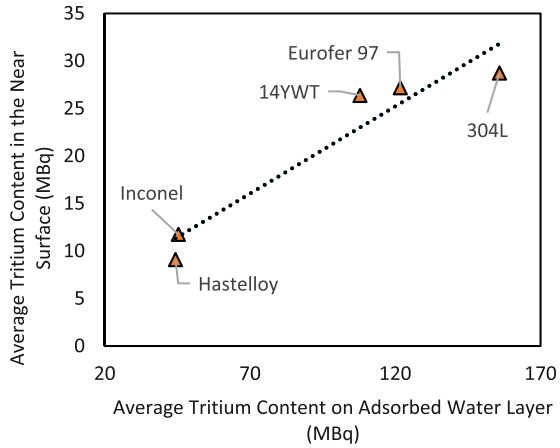

Fig. 7. Correlation between the quantity of surface bound tritium and the tritium in the "near surface" in the lower graph for the five alloys. The activity defined as in the near surface is the cumulative activity from all of the chemical etches.

B. XPS Characterization

XPS characterization has been completed for Hastelloy and AISI 304L and is shown in Fig. 8.

The iron content is on the order of 1% on the surface of Hastelloy and increases to 10% in the near surface. Iron content is on the order of 10% at the surface of AISI 304L. Oxygen exceeds 75% on both surfaces. Chromium is on the order of 8% at the Hastelloy and increases rapidly to 15% in the near surface. Chromium starts at 10% at the AISI 304L surface and increases to about 25% in the near surface. The chromium content and distribution are similar for the two alloys Hastelloy and AISI 304L.

C. EBSD Characterization

A preliminary EBSD was done (see Fig. 9) using an Oxford Instruments Symmetry S3 EBSD detector for the purpose of comparing these materials grain structure. These reveal the crystal orientations within the materials microstructure with respect to the different sample reference axes.

Table III shows the grain size and grain boundary measurements for the crystal orientation maps using the Oxford Instruments Aztec Crystal version 2.2. EBSD analysis software. The grain size reveals that both materials ferritic Eurofer and martensitic 14YWT grain sizes are 1/10 of the size of the austenitic steels Hastelloy, Inconel, and AISI 304L

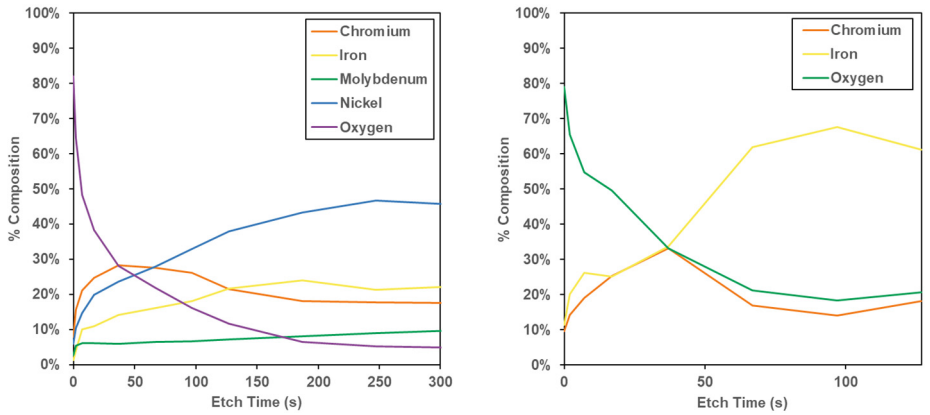

Fig. 8. XPS analysis of Hastelloy X (left figure) and AISI 304L (right figure).

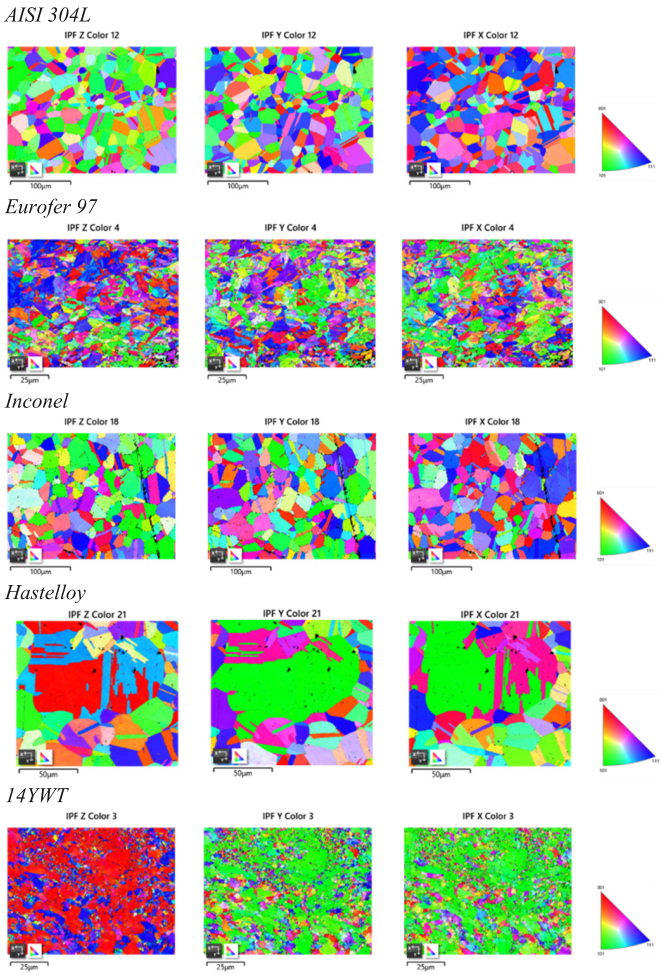

Fig. 9. EBSD patterns of the materials in this study. Miller indices are represented by red (111), green (101), and blue (111).

and possess much tighter grain size distribution. Eurofer and 14YWT arguably cannot be analyzed in this way and have been characterized in other literature [12], [18] and better equipment may be required. However, a full microstructural characterization is out of scope for this article.

IV. Discussion

A. Nickel-Based Alloys Absorbed Less Tritium Than Steels

The surface chemistry of tritium facing materials is important, and the water layers and oxide layers likely cause the tritium inventory in the material to deviate from classical diffusion [1], [2], [3], [4], [5], [6], [7], [8], [9].

The nickel-based alloys: Inconel X-750 and Hastelloy-X, absorbed the least average amount of tritium by comparison to the steels 14YWT, Eurofer97, or AISI 304L in each section of the tested materials; adsorbed water and deeper.

Reducing the iron content drastically with chromium at the surface has been shown to reduce tritium surface contamination [9], [19]. The XPS data confirm a lower iron content on the Hastelloy surface compared to 304L. XPS studies by others show iron suppression below 10% on the surfaces of Hastelloy and Inconel 625 [20]. Inconel X-750 and Inconel 625 are expected to behave similarly. The increased iron content on the surface is most likely responsible for the higher surface tritium content on 304L compared to Hastelloy X. It is expected that Eurofer97 and 14YWT are also steels that would exhibit

TABLE II

Color Quench Test Showing Minimal Error Is Expected From the Liquid Scintillation Due to Color

	Activity of Etchant Following Known Activity Spike (Disintegrations per minute (DPM))					
Spiked Activity (DPM)	Increasing Colour Saturation of Etchant					
	Lightest etchant					Darkest etchant
6.3E+06	6.3E+06	6.3E+06	6.4E+06	6.4E+06	6.4E+06	6.3E+06
64795	65000	66000	65000	64000	64000	64000
2086	2113	2059	2116	2151	2273	2100

TABLE III

EBSD Crystal Orientation Maps Grain Size and Boundary Analysis

	Grain Area (μm²)				
Material	**Grain Count**	**Min**	**Max**	**Mean**	**Std Dev**
AISI 304L	503	2.5	1814.79	411.89	185.18
Eurofer97	1066	1.0	98.21	24.8	11.4
Inconel	342	10	2080	483.55	229.7
Hastelloy	270	10	2401	746.14	336.95
14YWT	4634	0.1	493.23	85.52	12.1

similar iron contents at the surface. However, it should also be noted that the most corrosion resistant materials absorbed the least tritium.

Hydroxyl site density has been shown to depend on valency of the metal in the native metal oxide [21]. Chromium, iron, and nickel can have the same valency, although an increase in Fe(III) (magnetite) would result in an increase to the number of hydroxyl sites. Hydroxyl site density alone is not significant enough to explain the difference in tritium absorbed as nickel should behave broadly in a similar way to iron. There could be an alloying effect here which the authors are unsure of.

B. Microstructure Does Not Play a Dominant Role in This Type of Short-Term Exposure

The five alloys ordered by their grain size from largest to smallest are: Hastelloy, 304L/Inconel, Eurofer97, and 14YWT. The alloys ordered by tritium uptake are: Inconel/Hastelloy, 14YWT, Eurofer97, and 304L. Additionally, the grain orientation is not expected to influence absorption or diffusion greatly as outline by Youhan and Koehler [22].

Sink strength is a concept used to quantify microstructural features and their ability to absorb tritium [23]. Analysis [12] suggests that Eurofer 97 sink strength is on the order of 100 times less compared to 14YWT, assuming the trapping process is diffusion controlled. According to the sink strength concept, 14YWT should contain significantly more tritium than Eurofer 97. Figs. 5 and 6 indicate that the tritium inventory and depth profiles for both are similar. This shows that our data are not in the regime, where microstructural features related to sink strength are dominant. Our data are in the phase of uptake preceding this case.

V. Summary and Conclusion

Five alloys were exposed to tritium at 20 °C for 24 h: Inconel-X-750, Hastelloy-X, austenitic stainless steel AISI 304L, RAFM steel Eurofer-97, and nanoferritic alloy 14YWT. The nickel-based alloys Inconel X-750 and Hastelloy X absorbed the least quantity of tritium. Stainless steel AISI 304L absorbed the most. Alloy microstructure does not appear to play a dominant role in tritium uptake in these conditions. It is suggested that the drastic reduction of iron oxide dissolved in the metal oxide layer whether by chromium [9], [19] or nickel introduces a chemical effect, which will decrease the inventory of tritium on the surface of a material and subsequently in the alloy bulk. In a nonidealized environment—such as a tritium handling plant—this could be a useful way to reduce lost tritium inventory.

Acknowledgment

The authors would like to thank UR LLE staff for hosting UKAEA scientists at LLE and the UKAEA Materials Science and Engineering Group (MSE) for their support.

References

[1] A. Perevezentsev, K. Watanabe, M. Matsuyama, and Y. Torikai, "Contamination of stainless steel type 316 by tritium," *Fusion Sci. Technol.*, vol. 41, no. 3P2, pp. 746–750, May 2002, doi: 10.13182/fst02-a22686.

[2] A. N. Perevezentsev et al., "Study of tritium distribution in various metals," *Fusion Sci. Technol.*, vol. 48, no. 1, pp. 208–211, Aug. 2005.

[3] R.-D. Penzhorn et al., "Distribution and mobility of tritium in type 316 stainless steel," *Fusion Sci. Technol.*, vol. 57, no. 3, pp. 185–195, Apr. 2010, doi: 10.13182/fst57-3-185.

[4] M. Sharpe, "On the interaction of tritium with the surfaces of aluminum, copper, stainless steel (type 316), and gold," Ph.D. thesis, Univ. Rochester Lab. Laser Energetics, 2016.

[5] M. Sharpe, C. Fagan, and W. T. Shmayda, "Distribution of tritium in the near surface of type 316 stainless steel," *Fusion Sci. Technol.*, vol. 75, no. 8, pp. 1053–1057, Nov. 2019, doi: 10.1080/15361055.2019.1644136.

[6] M. D. Sharpe, C. Fagan, W. T. Shmayda, and W. U. Schröder, "Partitioning of tritium between surface and bulk of 316 stainless steel at room temperature," *Fusion Eng. Design*, vol. 130, pp. 76–79, May 2018, doi: 10.1016/j.fusengdes.2018.03.028.

[7] M. Sharpe, W. T. Shmayda, and W. U. Schräder, "Tritium migration to the surfaces of type 316 stainless steel; Aluminum 6061; And oxygen-free, high-conductivity copper," *Fusion Sci. Technol.*, vol. 70, no. 1, pp. 97–111, Jul. 2016, doi: 10.13182/fst15-198.

[8] C. Fagan, M. Sharpe, W. T. Shmayda, and W. U. Schröder, "A thin alumina film as a tritium adsorption inhibitor for stainless steel 316," *Fusion Sci. Technol.*, vol. 76, no. 4, pp. 424–429, May 2020, doi: 10.1080/15361055.2020.1714409.

[9] C. E. Fagan, "Tritium interactions with austenitic stainless steel type 316," Ph.D. thesis, Univ. Rochester Lab. Laser Energetics, 2021.

[10] B. Lynch, B. Normand, L. Président, R. Lindsay, and C. Blanc, "Oxide nucleation and growth mechanisms of a molybdenum-containing stainless steel and the effect of pre-oxidation on passive film behaviour," Ph.D. thesis, Chimie Physique et Chimie Analytique de Paris Centre, Paris Sci. et Lettres Univ., 2023.

[11] H. Izumi, Y. Nakagawa, S. Miyoshi, and T. Ohmi, "Measurement of adsorbed moisture concentration on various kinds of solid surfaces by using anhydrous hydrogen fluoride," in *Proc. Int. Symp. Semiconductor Manuf., Extended Abstr. (ISSM)*, Jun. 1994, pp. 211–212.

[12] X. Hu, L. Tan, K. Wang, C. P. Massey, D. T. Hoelzer, and Y. Katoh, "Deuterium retention in advanced steels for fusion reactor structural application," *J. Nucl. Mater.*, vol. 516, pp. 144–151, Apr. 2019, doi: 10.1016/j.jnucmat.2019.01.020.

[13] Y. Tanaka, H. Saito, Y. Tsutsumi, H. Doi, H. Imai, and T. Hanawa, "Active hydroxyl groups on surface oxide film of titanium, 316L stainless steel, and cobalt-chromium-molybdenum alloy and its effect on the immobilization of poly(ethylene glycol)," *Mater. Trans.*, vol. 49, no. 4, pp. 805–811, Apr. 2008, doi: 10.2320/matertrans.mra2007317.

[14] J. Borowski, M. Call, D. Dunn, A. Rigato, J. Smith, J. Solis, J. Tapp, and B. White, *Standard Review Plan for Transportation Packages for Spent Fuel and Radioactive Material: Final Report (NUREG-2216)*, document NUREG-2216, Regulatory Commission, Washington, DC, USA, Aug. 2020.

[15] P. A. Thiel and T. E. Madey, "The interaction of water with solid surfaces: Fundamental aspects," *Surf. Sci. Rep.*, vol. 7, nos. 6–8, pp. 211–385, Oct. 1987.

[16] R.-D. Penzhorn, Y. Torikai, M. Matsuyama, and K. Watanabe, "Detritiation of type 316 stainless steel by treatment with liquids at ambient temperature," *J. Nucl. Mater.*, vol. 353, nos. 1–2, pp. 66–74, Jul. 2006, doi: 10.1016/j.jnucmat.2006.03.004.

[17] A. B. Antoniazzi, W. T. Shmayda, and R. A. Surette, "Decontamination of stainless steel," *Fusion Technol.*, vol. 21, no. 2P2, pp. 867–871, Mar. 1992, doi: 10.13182/fst21-867.

[18] D. T. Hoelzer. (2019). *Materials Challenges for Advanced Reactors Systems*. IUPAC: Chemistry for Energy and Resources. [Online]. Available: http://www.gen-4.org/Technology/evolution.htm

[19] Y. Ozeki, Y. Hatano, H. Taniguchi, and M. Matsuyama, "Influence of chromium oxide layer on surface tritium contamination of type 316 stainless steel," *Fusion Sci. Technol.*, vol. 60, no. 4, pp. 1499–1502, Nov. 2011, doi: 10.13182/fst11-a12716.

[20] Y. Zhang et al., "Corrosion behavior and passive film properties of nickel-based alloy in phosphoric acid," *Corrosion Commun.*, vol. 9, pp. 77–88, Mar. 2023, doi: 10.1016/j.corcom.2022.06.003.

[21] H. Tamura, K. Mita, A. Tanaka, and M. Ito, "Mechanism of hydroxylation of metal oxide surfaces," *J. Colloid Interface Sci.*, vol. 243, no. 1, pp. 202–207, Nov. 2001, doi: 10.1006/jcis.2001.7864.

[22] U. K. Youhan and S. P. K. Koehler, "Energetics of hydrogen adsorption and diffusion for the main surface planes and all magnetic structures of γ-iron using density functional theory," *RSC Adv.*, vol. 11, no. 46, pp. 28892–28897, Aug. 2021, doi: 10.1039/d1ra04999b.

[23] L. K. Mansur, "Theory and experimental background on dimensional changes in irradiated alloys," *J. Nucl. Mater.*, vol. 216, pp. 97–123, Oct. 1994, doi: 10.1016/0022-3115(94)90009-4.